SAND2006-6176C
0207-01-2007

Thermodynamic and Chemical Effects of EGR and Its Constituents on HCCI Autoignition

Magnus Sjöberg, John E. Dec and Wontae Hwang
Sandia National Laboratories

ABSTRACT

EGR can be used beneficially to control combustion phasing in HCCI engines. To better understand the function of EGR, this study experimentally investigates the thermodynamic and chemical effects of real EGR, simulated EGR, dry EGR, and individual EGR constituents (N_2, CO_2, and H_2O) on the autoignition processes. This was done for gasoline and various PRF blends. The data show that addition of real EGR retards the autoignition timing for all fuels. However, the amount of retard is dependent on the specific fuel type. This can be explained by identifying and quantifying the various underlying mechanisms, which are: 1) Thermodynamic cooling effect due to increased specific-heat capacity, 2) [O_2] reduction effect, 3) Enhancement of autoignition due to the presence of H_2O, 4) Enhancement or suppression of autoignition due to the presence of trace species such as unburned or partially-oxidized hydrocarbons.

The results show that the single-stage ignition fuels iso-octane and gasoline are more sensitive to the cooling effect of EGR, compared to the two-stage ignition fuels PRF80 and PRF60. On the other hand, the two-stage ignition fuels have much higher sensitivity to the reduction of O_2 concentration associated with the addition of EGR. Furthermore, H_2O has a pronounced ignition-enhancing effect for the two-stage fuels that tends to counteract the strong cooling effect of H_2O. Finally, for the single-stage ignition fuels, gasoline and iso-octane, partially-oxidized fuel tends to enhance the ignition, thus counteracting the retarding effect of EGR. On the other hand, the trace species present for operation with the two-stage ignition fuel PRF80 increased the retarding effect of EGR.

In addition to the experiment, corresponding chemical-kinetics modeling was performed to evaluate the predictive capabilities of detailed iso-octane and PRF chemical-kinetics mechanisms from Lawrence Livermore National Laboratory (LLNL).

INTRODUCTION

The homogeneous charge compression ignition (HCCI) combustion process offers good fuel economy and very low nitrogen-oxide (NO_x) and particulate emissions. Therefore, engine manufacturers are considering HCCI combustion as one option to improve the efficiency of the traditional spark-ignited gasoline engine, and also to reduce NO_x aftertreatment requirement for traditional diesel engines. However, several technical difficulties need to be resolved before HCCI can be widely implemented in production engines. Among these, controlling the combustion phasing and increasing the power output while maintaining acceptable pressure-rise rates continue to be major issues.

The ignition quality of the fuel is an important parameter impacting the design of HCCI engines and the methods used to control the combustion phasing and the heat-release rate (HRR). HCCI operation has been demonstrated for a variety of fuels, whose autoignition qualities span a wide range [1,2,3,4]. However, recent HCCI development efforts have tended to focus on the use of gasoline and diesel fuels due to both their wide availability and because they provide the potential to revert to traditional spark-ignition (SI) or diesel combustion for high-load operation. Despite the large differences in the autoignition characteristics of these two fuels, virtually all applications for both fuels use some form of exhaust gas recirculation (EGR) to help control the combustion phasing and/or to provide other benefits at various parts of the operating map.

Because gasoline is a single-stage ignition fuel, the charge must be raised to a temperature on the order of 1050 K to achieve HCCI autoignition. Furthermore, most applications limit the compression ratio (CR) to about 12:1 to allow SI operation at high loads. To reach the required compressed-gas temperature with this modest CR, substantial quantities of hot residuals from the previous cycle are typically retained to heat the incoming charge. However, in addition to increasing the initial

charge temperature, these retained residuals (internal EGR) significantly alter the charge mixture composition and thermodynamic properties. These changes will tend to retard the combustion phasing, thus reducing the desired ignition enhancement caused by the high temperature of the retained residuals.

At higher loads, less internal EGR is required due to the higher temperature of the residuals and the increased in-cylinder surface temperatures [5]. However, these higher fueling rates can produce combustion temperatures that are sufficiently high to produce NO_x emissions that would be unacceptable without aftertreatment. To allow the use of a three-way catalyst to remove this NO_x, it can be desirable to operate with a stoichiometric charge, using high levels of EGR to dilute the charge sufficiently to maintain acceptable heat-release rates. Accomplishing this, while maintaining the desired combustion phasing, typically requires that cooled external EGR be combined with retained hot residuals [6]. Thus, the use of substantial EGR/residuals is central to most gasoline HCCI applications, and it is important to understand the effects of this EGR on the combustion phasing.

In contrast, diesel fuel autoignites quite easily under HCCI-like conditions due to its strong low-temperature heat release (LTHR) or "cool-flame" chemistry. This can lead to overly advanced combustion phasing and/or require a substantial reduction in the allowable CR [7]. Since neither of these is particularly desirable from an engine-design standpoint, most diesel-fueled HCCI engines use substantial quantities of EGR to reduce the autoignition propensity of the fuel. In addition, most diesel HCCI-like applications rely on direct-injection to supply the fuel after compression has raised the temperature and pressure of the charge sufficiently to readily vaporize the low-volatility fuel. However, supplying the fuel in this manner limits the time for vaporization and mixing before ignition occurs. Substantial EGR addition is typically employed to increase the ignition delay to allow sufficient time for fuel/charge mixing. Finally, despite this increased mixing time, some regions can still remain sufficiently close to stoichiometric that unacceptable NO_x formation could occur. However, the use of EGR reduces the oxygen concentration sufficiently so that peak combustion temperatures in these regions do not reach those required for significant NO_x formation [8]. Thus, the use of EGR is also central to diesel HCCI combustion, and it is important to understand its effect on combustion phasing for these two-stage ignition fuels.

In addition to these traditional fuels, two-stage ignition fuels that have less LTHR than diesel fuel and a higher volatility have recently been investigated and shown to offer four advantages for combustion-phasing control and extending high-load HCCI operation [5,9,10]. It may also be possible to achieve these results with other two-stage fuels such as diesel fuel; however, the higher volatility and lower amount of LTHR of the fuels used facilitated mixture formation and implementation of the control methods. A detailed discussion of these four advantages is provided in Ref. [10]. A brief summary follows:

1. Because the amount of LTHR produced by a two-stage fuel increases with the local fuel/air-equivalence ratio (ϕ), fuel stratification can be used for combustion-phasing control [5,9,11]. This allows near-instantaneous control of combustion phasing during transients since the amount of stratification can be varied by changes in injection timing [5].
2. This ϕ-dependence of the LTHR also provides a means for reducing the peak HRR. In Ref. [9], a dual-injection scheme was used to create a range of local equivalence ratios in the combustion chamber, which resulted in a staged autoignition/combustion event, increasing the burn duration and reducing the peak HRR.
3. With two-stage fuels, the engine has lower cycle-to-cycle variations when operated with extensive combustion-phasing retard because the LTHR leads to higher temperature-rise rates just prior to hot ignition [12]. This could allow higher loads without engine knock since increased combustion-phasing retard produces significant reductions in the HRR [13,14,15].
4. With LTHR, lower intake temperatures (T_{in}) are required. This results in a greater mass inducted for a fixed intake pressure, and can potentially enable higher engine loads.

Although two-stage ignition fuels offer these potential advantages, realizing them in a practical application requires that the amount of LTHR be controlled over the load-speed map of the engine. This is challenging because the amount of LTHR is not only a property of the fuel, but it is also dependent on the operating conditions. For example, the LTHR can vary substantially as the engine speed is varied [10,11,16]. This is demonstrated for three primary reference fuel (PRF) blends in Fig. 1b (reproduced from [10]). PRF90, PRF80 and PRF70 were all operated with only normal air dilution, and the combustion phasing (CA50) was held fixed at 372°CA by adjusting T_{in} as the engine speed was changed. As Fig. 1b shows, T_{in} had to be increased rapidly with increasing engine speed. As indicated by the dashed line, above a certain engine speed, the LTHR disappears. This happens because LTHR is a slow combustion process and an increase of the engine speed leads to a reduction of the time spent in the temperature range that favors LTHR (760 – 880 K), thus reducing the amount of LTHR. To compensate for the lower temperature rise during the compression stroke, T_{in} was increased. Unfortunately, the increased T_{in} also disfavors LTHR since it leads to lower pressure in the 760 – 880 K range (see Figs. 4 and 5 in Ref. [10]). The compounding effect of less time and higher T_{in} makes the LTHR disappear quickly. The loss of LTHR effectively makes the fuel a single-stage ignition fuel, with an associated loss of the benefits listed above. Conversely, if the engine speed is reduced, the required T_{in} can drop below ambient, which is clearly impractical.

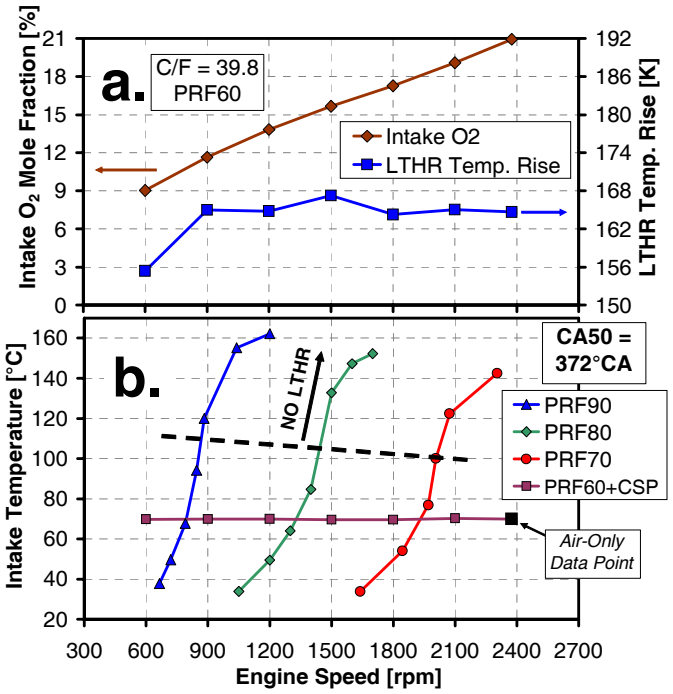

Figure 1. Required T_{in} as a function of engine speed for operation without CSP (EGR) addition for PRF90, PRF80 and PRF70, and with CSP addition for PRF60. Intake O_2 concentration and LTHR-temperature rise (335 - 352°CA) are plotted for the PRF60 case. C/F-mass ratio = 39.8, corresponding to ϕ = 0.38 for operation without CSP. Reproduced from [10].

To overcome this problem, it is necessary to manage the amount of LTHR as the speed is varied. This has been explored in Ref. [10], and as shown in Fig. 1, EGR addition provides an effective method for controlling the amount of LTHR over a wide range of engine speeds. For the example in Fig. 1, this was accomplished by using a fuel that was reactive enough to produce LTHR at the highest engine speed of interest (PRF60), and then suppressing the excessive LTHR at lower engine speeds by applying EGR. For this study, EGR was simulated by adding complete stoichiometric products (CSP), *i.e.* N_2, CO_2 and H_2O in amounts proportional to the complete combustion of PRF60. Fig. 1a shows how the CSP addition reduced the intake O_2 concentration and that this led to a nearly constant amount of LTHR. Accordingly, no T_{in} adjustment was required to maintain a constant CA50 over the speed range. [1]

Since EGR is effective for managing LTHR for this two-stage fuel blend, the potential exists to use the benefits of LTHR for combustion-phasing and HRR control over a wide range of engine speeds. Similarly, EGR could be used to control LTHR variations due to changes in other engine parameters such as intake boost pressure. Moreover, the use of EGR/residuals is central to virtually all current practical gasoline- and diesel-fueled applications of HCCI, as discussed above. This provides a strong motivation to investigate the underlying mechanisms that lead to the observed influences of EGR on HCCI combustion phasing for both single- and two-stage ignition fuels.

Finally, it should be noted that during the design process of advanced HCCI engines, CFD modeling is often employed to provide insights and to speed up the development. However, the quality of the modeling hinges on the fidelity of the chemical-kinetics models employed. Consequently, there is also a need to investigate the accuracy of chemical-kinetics mechanisms for operation with EGR.

SCOPE AND OBJECTIVES

The main objective of this study is to experimentally investigate the effect of EGR addition on the onset of combustion, and to clarify the underlying mechanisms for both single- and two-stage ignition fuels. The fuels considered are gasoline, iso-octane, PRF80 and PRF60.

Following the description of the model and the experiment, this paper covers five main areas:

1. The basic considerations regarding simulated EGR and real EGR are laid out.
2. It is demonstrated that the retarding effect of EGR varies with both fuel-type and type of EGR.
3. For motored operation, the thermodynamic effect of EGR and its major constituents is quantified.
4. For fired operation, it is shown how the retarding effect of EGR can be divided into thermodynamic and chemical effects. It is illustrated how the relative importance of the thermodynamic and chemical effects changes with fuel-type. The different effects of the trace species in real EGR are demonstrated and discussed.
5. Finally, the thermodynamic library used for the chemical-kinetics modeling is validated, and the performance of the chemical-kinetics mechanisms for iso-octane and PRF from Lawrence Livermore National Laboratory (LLNL) is compared against experimental data

CHEMICAL-KINETICS MODELING SETUP

The chemical-kinetic modeling approach used in this work is similar to that used previously by the authors [5,11,12,17]. This approach employs the Senkin application of the CHEMKIN-III kinetics rate code [18], which treats the in-cylinder charge as a single lumped mass with uniform composition and thermodynamic properties (single-zone model). The most current reaction mechanism from LLNL was used for iso-octane [19]. The PRF mechanism contains the same iso-octane

[1] As will be discussed later in this paper, CSP addition with a two-stage ignition fuel affects both the LTHR reactions and the reactions leading up to the main hot ignition. Thus, the constant CA50 with constant T_{in} demonstrated in Fig. 1 results from a combination of a nearly constant LTHR [10] and a suppression of the reactions leading to hot ignition.

mechanism combined with the most recent LLNL *n*-heptane mechanism [20] with updates to make it consistent with the newer iso-octane mechanism [21]. For simplicity, heat transfer effects were not modeled. However, to ensure the same charge-pressure history during the compression stroke, the model was set up with CR = 12.7, which is slightly lower than the CR = 14 used in the experiment.

The air was modeled using only N_2 and O_2 with a molecular ratio of 3.773 to 1, where atmospheric argon and CO_2 have been lumped as atmospheric N_2, following Ref. [22]. EGR was modeled using the correct proportions of CO_2, H_2O, N_2 (CSP), and air. For this modeling work, no attempt was made to capture the effect of trace hydrocarbon species encountered experimentally in real EGR. For the EGR sweeps, air was replaced by CSP or the individual constituents, while the fueling rate was adjusted to maintain a constant charge/fuel mass ratio of 37.8, which corresponds to ϕ = 0.40 for operation with air dilution only.

EXPERIMENTAL SETUP

The engine used for this study is based on a Cummins B-series diesel engine, which is a typical medium-duty diesel engine with a displacement of 0.98 liters/cylinder. The configuration of the engine and facility is nearly the same as for previous studies [5,9-15,17]. A schematic of the setup is shown in Fig. 2. For all operating conditions, the engine was fueled using a fully-premixed fueling system featuring an external electrically-heated fuel vaporizer. In addition to the existing air nozzle, metering nozzles for CO_2 and N_2 were installed. To supply H_2O to the intake charge, a metering pump was used to draw water from a bottle placed on a digital scale and feed it into the fuel vaporizer. A CR = 14 piston was installed for these tests, and the resulting combustion-chamber geometry at TDC is also pictured in Fig. 2. This custom-design piston provides a small topland-ring crevice, amounting to only 2.1% of the top-dead-center (TDC) volume, including the volume behind the top piston ring. An air heater mounted close to the engine was used to precisely control the intake temperature. Engine specifications are listed in Table 1. A detailed description of the engine modifications for HCCI operation can be found in Ref. [17].

TABLE 1. Engine Specifications

Displacement (single-cylinder)	0.981 liters
Bore	102 mm
Stroke	120 mm
Connecting Rod Length	192 mm
Nominal Geometric Compression Ratio	14:1
No. of Valves	4
IVO	717°CA*
IVC	205°CA*
EVO	480°CA*
EVC	8°CA*
Intake Air Swirl Ratio, Both Ports Combined	0.9

* 0°CA is taken to be TDC intake, so TDC combustion is 360°CA.

Cylinder pressure measurements were made with a transducer (AVL QC33C) mounted in the cylinder head approximately 42 mm off center. The pressure

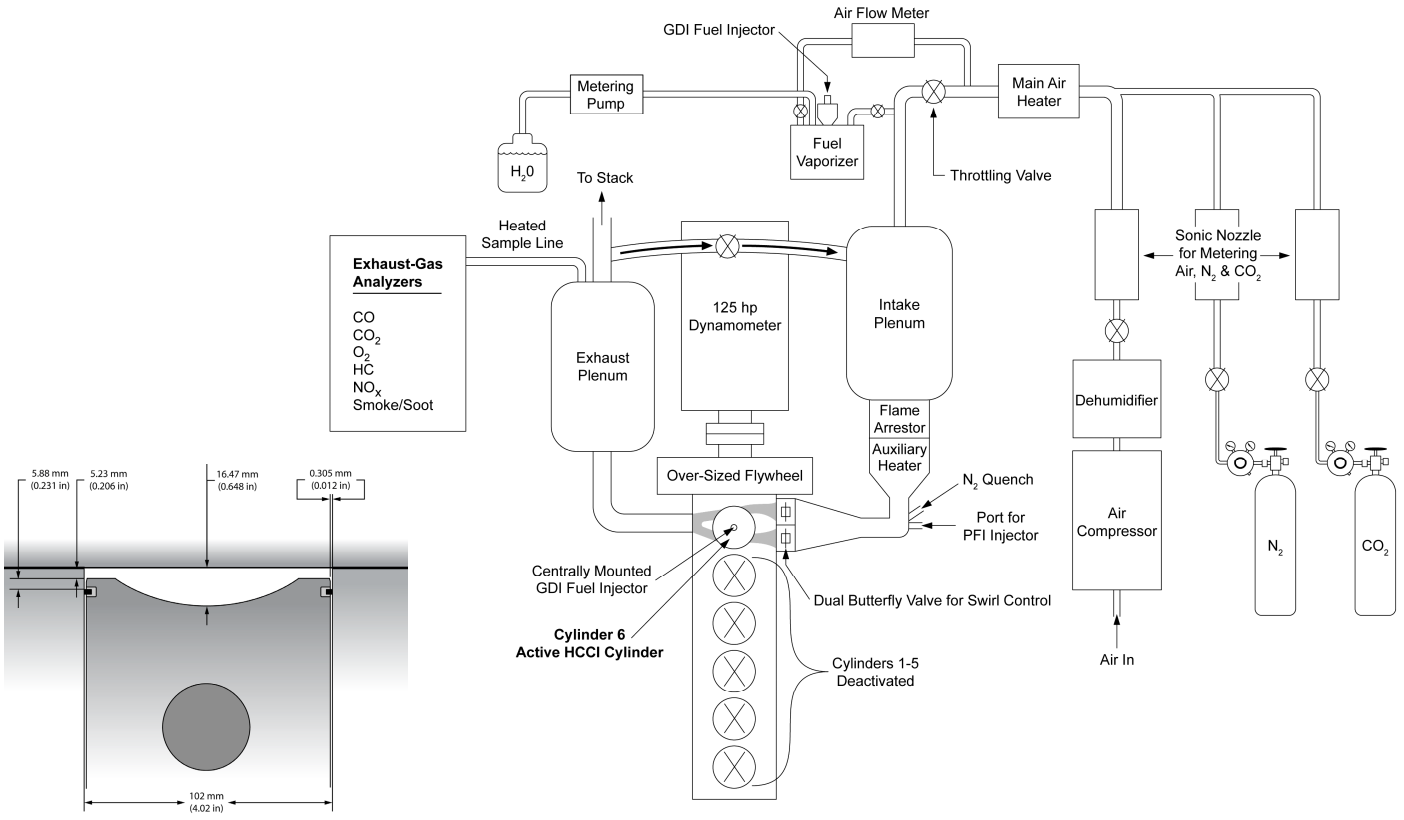

Figure 2. Schematic of the HCCI engine facility, and combustion-chamber dimensions at TDC with the CR = 14 piston.

TABLE 2. Fuel Properties

Fuel	Iso-Octane	PRF80	PRF60	Gasoline
Iso-Octane %vol.	100	80	60	Unknown
n-Heptane %vol.	0	20	40	Unknown
Saturates %vol.	100	100	100	73.4
Olefins %vol.	0	0	0	4.1
Aromatics %vol.	0	0	0	22.5
RON	100	80	60	90.8
MON	100	80	60	83.4
Antiknock Index (R+M)/2	100	80	60	87.1
C-atoms	8	7.78	7.57	6.83
H-atoms	18	17.56	17.14	13.08
Molecular weight	114.23	111.15	108.21	95.2
A/F Stoichiometric	15.13	15.14	15.15	14.66
Lower heating value for gas-phase fuel [MJ/kg]	44.65	44.71	44.76	43.52
Lower heating value for stoichiometric charge [MJ/kg]	2.769	2.770	2.772	2.779

Gasoline data provided by Chevron Phillips Chemical Co.

transducer signals were digitized and recorded at ¼°CA increments for 100 consecutive cycles. The 10% burn point (CA10) was first computed for each individual cycle (without heat-transfer correction), and then averaged. However, it should be noted that for operation with the presence of LTHR, the low-temperature heat release is excluded when the cumulative heat release is computed. Effectively, the reported combustion phasings refer to CA10 for the main combustion event, starting at the crank angle of minimum heat-release rate between the low- and high- temperature combustion events. Presenting the data referring to the main combustion event alone is considered more relevant from the standpoint of quantifying the onset of the main combustion event. It also eliminates the need to correct for heat transfer during the weak low-temperature combustion phase which extends for many crank angles. This makes the data acquisition faster and more consistent between engine operators.

The temperatures during the compression stroke, as reported here, are computed using the ideal-gas law in combination with the measured pressure (ensemble-averaged over 100 cycles), the known cylinder volume, and the trapped mass. The average molecular weight used for the calculation corresponds to that of the fresh gases inducted, including EGR or individual EGR constituents, and the fuel.

The fuels used were gasoline and blends of the primary reference fuels (PRF), iso-octane and *n*-heptane. The PRF blends allow selection of autoignition reactivity by varying the blending proportions. They are also fairly volatile, and this facilitates the charge preparation. Table 2 shows the fuel compositions and other relevant parameters.

Because HCCI combustion is very sensitive to temperature, the engine coolant and oil were both fully preheated to 100°C before starting the experiments. At each operating point, the engine was allowed to run for several minutes until all measured parameters were stable, at which point the data were acquired. For all data presented, 0° crank angle (CA) is defined as TDC intake (so TDC compression is at 360°). This eliminates the need to use negative crank angles or combined bTDC, aTDC notation.

BASIC EGR CONSIDERATIONS

In an engine operating lean with complete combustion, EGR consists of air and complete stoichiometric products (CSP). Typically there are combustion inefficiencies, and this generates trace species like carbon monoxide (CO), hydrocarbons (HC) and partially-oxidized hydrocarbons that can influence the autoignition. To separate the various effects of real EGR, this study also uses simulated EGR and its individual constituents. The simulated EGR consists of a mixture of air with the three main components of complete stoichiometric products (CSP), namely CO_2, H_2O and N_2. However, the relative proportions of these components vary with fuel-type and can be computed based on the average number of C and H atoms listed in Table 2. For iso-octane, complete stoichiometric combustion can be written as:

$$C_8H_{18} + 12.5\ (O_2 + 3.773\ N_2) \Rightarrow 8\ CO_2 + 9\ H_2O + 47.16\ N_2$$

where atmospheric argon and CO_2 have been lumped into the atmospheric N_2, following Ref. [22]. For complete combustion with ϕ = 1, the gas composition (excluding fuel) changes from: 20.95% O_2 and 79.05% N_2 for intake air, to products with 12.47% CO_2, 14.03% H_2O and 73.50% N_2 for wet exhaust. This exhaust composition will be referred to as CSP. As Table 3 shows, the CSP composition varies little with changes in PRF number. However, gasoline has significantly higher CO_2 mole fraction, *i.e.* [CO_2], and lower [H_2O] due to its lower H/C ratio. Table 3 also shows the composition of

TABLE 3. Composition of CSP and dry CSP for all four fuels (% mole fraction). Average molecular weight (M) and H/C ratio are also given.

Fuel:	Iso-Octane		PRF80		PRF60		Gasoline	
Gas:	CSP	Dry CSP	CSP	Dry CSP	CSP	Dry CSP	CSP	Dry CSP
CO_2	12.47	14.50	12.45	14.49	12.44	14.47	13.27	15.20
H_2O	14.03	0.00	14.05	0.00	14.08	0.00	12.71	0.00
N_2	73.50	85.50	73.49	85.51	73.48	85.53	74.03	84.80
M	28.71	30.46	28.71	30.46	28.70	30.45	28.97	30.57
H/C	2.25		2.26		2.26		1.92	

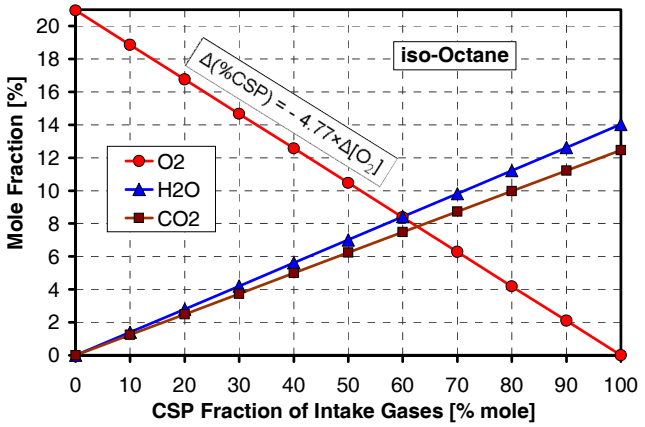

Figure 3. Intake mole fraction of O_2, CO_2, and H_2O as a function of CSP mole fraction. Iso-octane. Excluding fuel.

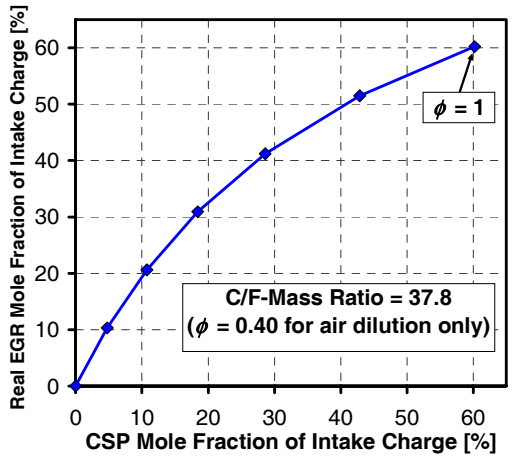

Figure 4. Relationship between the mole fraction of real EGR in the intake system and the intake CSP mole fraction (excluding fuel). C/F-mass ratio = 37.8. Iso-octane.

dry CSP, which represents the extreme case of complete water condensation before the exhaust gases are introduced into the intake system. As can be seen, dry CSP has significantly higher mole fractions of both CO_2 and N_2.

To simulate various amounts of EGR, air and CSP (CO_2, H_2O, N_2) were metered into the intake system to form a homogeneous mixture. Figure 3 demonstrates how the intake gas composition changes with CSP mole fraction. The mole fractions of CO_2 and H_2O ([CO_2] and [H_2O]) both increase linearly with increasing fraction of CSP, while [O_2] decreases linearly. As will be shown in the results section, O_2 concentration directly influences the autoignition reactions, regardless of the type of diluent. Therefore, all data will be plotted against [O_2] instead of CSP mole fraction. For all these graphs, the given [O_2] can be converted to the approximate CSP mole fraction by using Fig. 3. Also, as annotated in the graph, a reduction of [O_2] by one percentage unit corresponds to 4.77% increase of the CSP mole fraction. The same relationship holds for any diluent that does not contain O_2.

Since practical engines will incorporate real EGR, it is useful to also examine the relationship between the real EGR recirculation rate and the resulting intake CSP fraction. This is shown in Fig. 4 for the charge[2]/fuel-mass ratio (C/F) of 37.8 used in this study[3]. As can be seen, the real EGR fraction is higher than the CSP fraction, except for stoichiometric combustion. This happens because the exhaust from lean operation also contains "unused" air, in addition to combustion products.

It should be noted that the relationship between the intake CSP fraction and the real EGR recirculation rate varies with the actual fueling rate, so Fig. 3 cannot be used for C/F values other than 37.8. However, all data in this study (except for Figs. 1 & 22) were acquired with a C/F-mass ratio of 37.8, which corresponds to ϕ = 0.40 for operation without EGR. Finally, it can be noted from Table 3 that the average molecular weight of CSP is similar to that of air, 28.96 g/mol. Because of this, the CSP mass fraction is similar to the CSP mole fraction. Consequently, stoichiometric operation with a C/F-mass ratio of 37.8 requires that both the mole and mass fraction of exhaust present in the intake be close to 60%.

EXPERIMENTAL RESULTS

The engine speed was kept at 1200 rpm throughout the study. For all data with CSP, CO_2, H_2O or N_2 addition, the intake pressure (P_{in}) was maintained at 100 kPa, simulating naturally aspirated operation. For operation with real EGR, $P_{in} \approx$ 98 – 99 kPa, depending on the actual atmospheric pressure during the experiment. This happens because with the EGR passage open, the pressure in the intake system is dictated by the exhaust back pressure. The amount of real EGR is adjusted by changing the metered flow of air. With a reduction of air flow, more exhaust is inducted via the EGR passage.

AUTOIGNITION-REACTIVITY CONSIDERATIONS

As outlined above, this study investigates the effect of EGR addition on the combustion phasing of four fuels. For each fuel, a baseline operating point was first established. This section explains how this was done.

Plotted in Fig. 5b is the T_{in} required to position the 50% burn point (CA50) at 368°CA as a function of the PRF number (anti-knock index for gasoline). As can be seen, iso-octane (PRF100) and gasoline both require relatively high T_{in}. This happens because these two fuels both exhibit single-stage ignition at these operating conditions[4]. On the other hand, PRF80 and PRF60 exhibit two-stage ignition with LTHR for these operating conditions. As Fig. 6b shows, the LTHR accelerates the temperature rise towards the end of the compression

[2] The charge mass is the sum of the supplied air and CSP constituents, excluding the fuel.
[3] The C/F-mass ratio was somewhat higher (39.8) for Fig. 1 and slightly lower (36.9) for Fig. 22.
[4] As shown in Refs. [2] and [23], both iso-octane and gasoline can exhibit two-stage ignition with LTHR under conditions of elevated intake pressure.

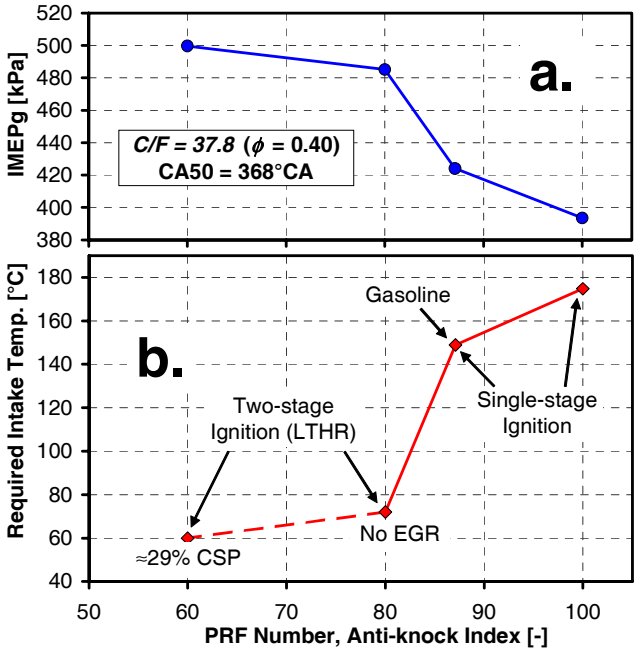

Figure 5. $IMEP_g$ and required T_{in} as a function of PRF number and anti-knock index for operation with air dilution only for iso-octane, gasoline, and PRF80, and with ≈29% CSP addition for PRF60. 1200 rpm. C/F-mass ratio = 37.8, corresponding to ϕ = 0.40 with air dilution.

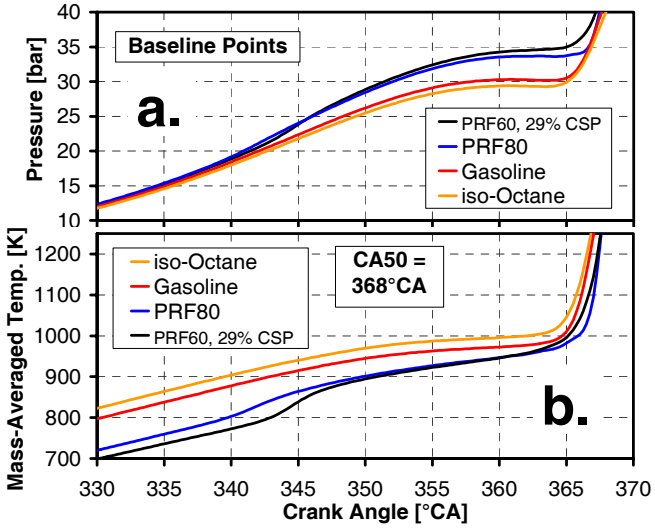

Figure 6. Pressure and temperature traces for each fuel's baseline operating point.

stroke. Therefore, T_{in} has to be reduced to achieve the same CA50. In the case of PRF80, Fig. 5 shows that it is sufficient to drop T_{in} to 72°C. However, PRF60 is so reactive that without EGR it would have been necessary to drop T_{in} well below ambient to maintain a constant CA50, which is not practical. Instead, ≈29% of the air was replaced with CSP while T_{in} was set to 60°C to avoid condensation of water in the intake system. As evident in Fig. 6, this CSP addition makes both the temperature and pressure rise associated with LTHR comparable for the two PRF blends. Furthermore, Fig. 5a shows how the $IMEP_g$ varies between these fuels. PRF60 exhibits the highest power output and iso-octane the lowest. This happens because P_{in} was maintained at 100 kPa while the C/F-mass ratio = 37.8. Since higher T_{in} lowers the charge density, less fuel will be inducted, as mentioned in the introduction (bullet #4).

AUTOIGNITION RETARD WITH EGR

The main purpose of this study is to explain the underlying mechanisms responsible for the combustion-phasing retard that is observed for EGR addition under conditions of constant T_{in}. To start out, this section illustrates the retarding effect of EGR. For the data sets presented below, EGR was added progressively until the combustion became unstable. As a result, the most retarded point for each data set typically has a standard deviation of CA10 on the order of 1.2°CA for the single-stage ignition fuels, and 0.7°CA for the two-stage ignition fuels. This can be compared with the more stable baseline points with CA10 variations on the order of 0.45°CA and 0.25°CA, respectively.

Figure 7 shows how the start of combustion measured here as CA10 becomes retarded by addition of CSP. CA10 is chosen since the purpose of this study is to study the effect of EGR on the autoignition timing. (CA50 would be a better measure of engine performance. However, CA50 is dependent on both the autoignition timing and the burn duration. The latter can be influenced by both EGR and combustion phasing, so choosing CA50 would make the trends more complicated to explain.) For reference, a reduction of the intake $[O_2]$ by one percentage unit corresponds to increasing the CSP mole fraction by 4.77 percentage units, as discussed in conjunction with Fig. 3. The retarding effect of CSP is strong for all fuels investigated, as Fig. 7 shows. However, it is difficult to compare PRF60 with the other fuels since its baseline point was established with 29% CSP, as explained above. To facilitate such comparison, the data are replotted on an expanded scale in Fig. 8, but now with the PRF60 data set shifted 6.1% $[O_2]$ to the left[5]. As can be seen, the effect of CSP is strong for all fuels, but there are also significant differences. The strongest effect is seen for pure iso-octane, while the fuel with the lowest sensitivity to CSP addition is gasoline. This is an interesting finding, especially since iso-octane is often used as a single-component surrogate for gasoline. Furthermore, Fig. 8 shows that PRF80 and PRF60 fall in between iso-octane and gasoline. It is also noteworthy that PRF60's sensitivity to CSP addition is similar to PRF80's, despite the fact that PRF60's baseline point was established with 29% CSP. This indicates that the effect of CSP addition is not saturated at PRF60's baseline point. Because PRF60's behavior is very similar to that of PRF80, PRF60 will not be presented in all graphs below.

[5] To facilitate comparison, the data sets in Fig. 8 have also been adjusted slightly (≈0.8°CA) vertically to make the baseline $[O_2]$ = 20.95% points coincide for the different fuels. This was necessary because the baseline CA50 was set to 368°CA and CA10 varies slightly between the fuels due to variations in the burn duration. This adjustment was also done for subsequent figures where different fuels are compared.

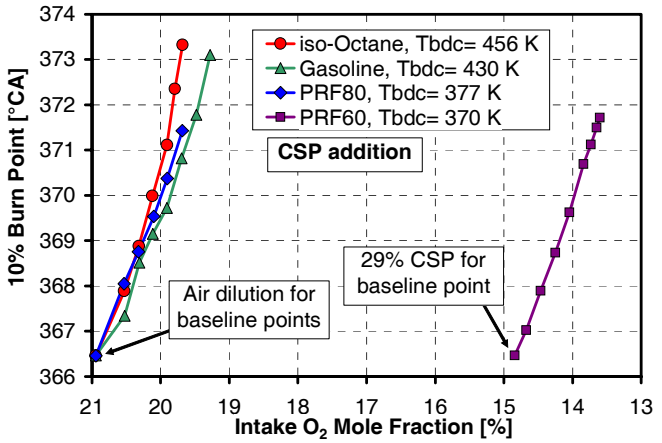

Figure 7. Effect of CSP addition on the start of combustion, measured as CA10.

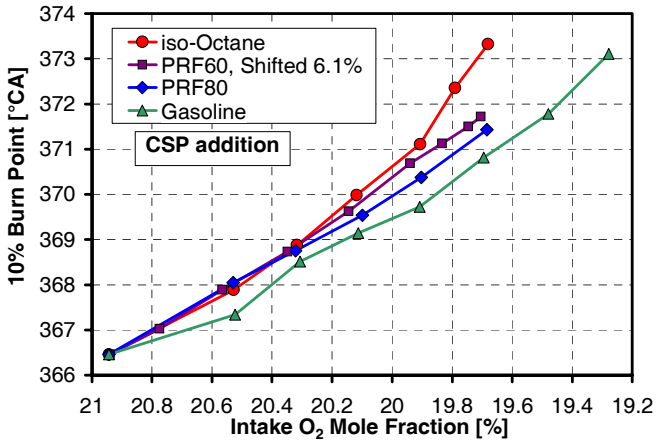

Figure 8. The data from Fig. 7, but with the PRF60 data set shifted 6.1% to facilitate direct comparison of the fuels.

In practical applications of EGR, the recirculated gases contain species like unburned fuel, partially oxidized fuel and CO, in addition to the major species CO_2, H_2O, N_2, and O_2. These trace species can have significant effects on the autoignition processes. This is illustrated in Fig. 9, which shows the retarding effect of real EGR. Comparing Figs. 8 and 9, it can be seen that the use of real EGR changes the relative sensitivities of the fuels. For example, PRF80 is more sensitive to real EGR than iso-octane, whereas the opposite was observed for CSP. This will be examined in greater detail later in the paper.

Finally, in practical EGR systems, the water content in the exhaust may condense onto cold surfaces, especially during cold weather and/or cold starting. Such condensation will change the composition of the EGR gases and potentially also its influence on the combustion phasing. The effect is illustrated for iso-octane and PRF80 in Fig. 10. Loss of water makes CSP less effective for iso-octane, whereas the opposite is observed for PRF80.

Taken together, the results presented in Figs. 8 – 10 provide motivation to clarify the underlying mechanisms responsible for the combustion-phasing retard observed

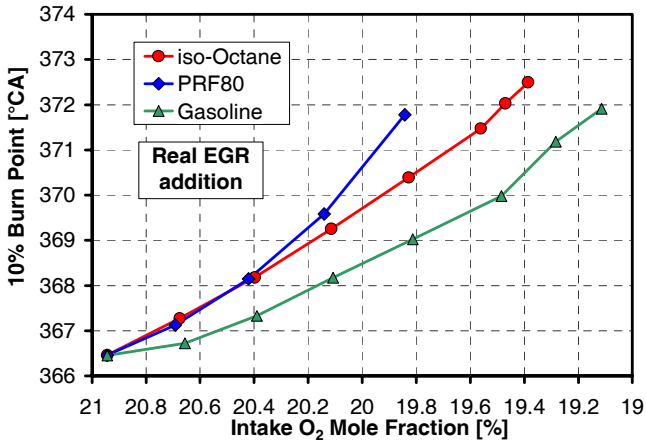

Figure 9. Effect of real EGR addition on CA10. Iso-octane, PRF80 and gasoline.

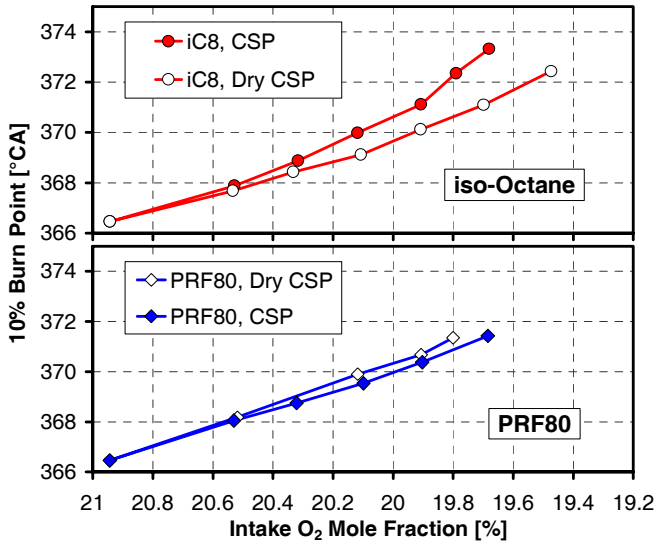

Figure 10 Effect of CSP and dry CSP addition on CA10. Iso-octane and PRF80.

for the different fuels. As these results suggest, there are both thermodynamic and chemical effects responsible for the observed combustion-phasing retard.

THERMODYNAMIC EFFECT OF EGR

To serve as a fundament for the following sections, motored data are presented here to clearly show the thermodynamic effect of EGR. Motored operation has the advantage of no heat-releasing reactions, and therefore nearly constant wall and residual temperatures. This allows the effects of CSP and its constituents on the compressed-gas temperature to be evaluated. The engine was operated with T_{in} = 100°C, which equals the coolant temperature. This minimizes heat transfer during the induction stroke. While maintaining P_{in} = 100 kPa, air was progressively replaced with increasing amounts of CSP or its individual constituents. The resulting changes of the compressed gas temperature are shown in Fig. 11.

The mass-averaged compression temperature at 350°CA (T_{350}) is 888 K for operation with air dilution only,

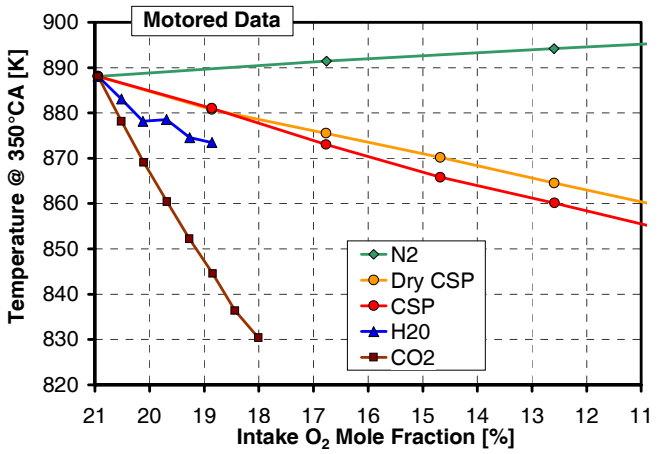

Figure 11. Effect of addition of CSP and constituents on compressed gas temperature at 350°CA (10°CA before TDC). T_{in} = 100°C.

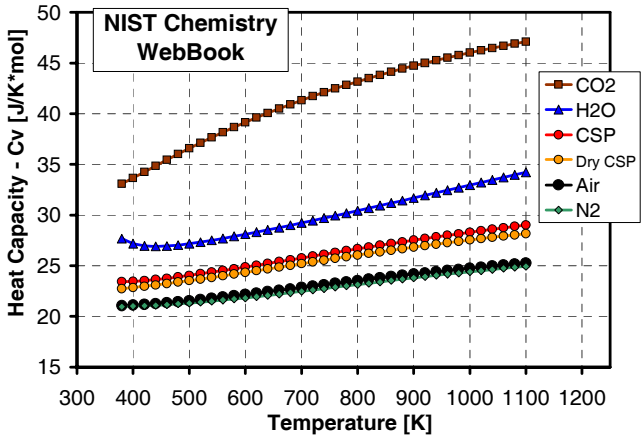

Figure 12. Mole-specific heat capacity as a function of temperature for air, CSP and CSP constituents. Data from NIST Chemistry WebBook [24]. The data corresponds to a pressure of 20 bar, except for H_2O which is for 1 bar. (H_2O is a liquid below 486 K at 20 bar.)

i.e. with $[O_2]$ = 20.95%. As Fig. 11 shows, replacing air with EGR or its constituents always leads to a change in the compressed-gas temperature. For example, replacing 40% of the air with CSP reduces $[O_2]$ to 12.6% and lowers T_{350} to 860 K. The strongest cooling effect is found for CO_2, and it takes only 14% CO_2 (making $[O_2]$ drop to 18.0%) to make T_{350} drop to 830 K. The cooling effect of H_2O falls in between CO_2 and CSP. Furthermore, when the water is removed from CSP to produce dry CSP, the cooling effect is reduced. It is noteworthy that addition of N_2 has the opposite effect and actually increases the compressed-gas temperature slightly.

The trends in Fig. 11 can be explained by considering the changes of the mole-specific heat capacity (C_v) that occur with addition of these gases. Figure 12 shows C_v as a function of temperature for all the gases presented in Fig. 11. CO_2 stands out with a C_v that is roughly 80% higher than that of air, and this explains the strong cooling effect of CO_2, as shown in Fig. 11. For a higher C_v, more energy (compression work) is required to raise the charge temperature a certain amount. In addition, because of lower compression pressures caused by lower gas temperatures, the total piston-compression work tends to decrease slightly when C_v increases. The net result of the higher C_v and the slightly lower compression work is a significant reduction of the compressed-gas temperature. The high C_v of CO_2 can be explained partly by the fact that CO_2 is a tri-atomic molecule with more vibrational and rotational modes compared to the di-atomic N_2, which is the major constituent in air. H_2O is also a tri-atomic molecule with C_v higher than air. However, its C_v is not as high as that of CO_2. Comparing Figs. 11 and 12, it can be seen that changes of C_v fully explain the trends of compression temperature. Specifically, it can be noted that N_2 has slightly lower C_v than air, which explains the somewhat increased compression temperatures shown in Fig. 11. Furthermore, dry CSP has a lower C_v than CSP because the H_2O was removed. This explains the higher compressed-gas temperature for dry CSP.

COMBUSTION RETARD FOR ISO-OCTANE

To fully understand the differences between the fuels as demonstrated in Figs. 8 – 10, the following sections will examine the underlying mechanisms for each fuel separately. This particular section presents detailed results for iso-octane, which has single-stage autoignition for the operating conditions studied here.

The effects of addition of CSP, dry CSP and individual constituents are plotted in Figs. 13a and 13b, which only differ by the scaling of the x-axis. First, it can be observed that addition of N_2 leads to a retard of CA10. This happens despite the fact that N_2 addition tends to increase the compressed-gas temperature slightly, as was discussed with respect to Fig. 11. The only plausible explanation is that the autoignition reactions are sensitive to $[O_2]$, despite the abundance of O_2 for these lean operating conditions. This finding is in agreement with rapid-compression experiments by He *et al.* [25]. This $[O_2]$ effect is expected to be present for all gases, but since N_2 is the only gas that does not reduce the compressed-gas temperature, only N_2 can be used to separately quantify the $[O_2]$ effect[6]. However, it is assumed that the $[O_2]$ reduction effect influences all gas mixtures equally. Consequently, for all other gases, the observed CA10 retard results from a combination of thermodynamic cooling and the $[O_2]$ effect. Comparing the slopes of the curves, it can be concluded that within the range of air displacement plotted in Fig. 13b, the $[O_2]$

[6] Motored data in Fig. 11 show that N_2 addition actually increases the compressed-gas temperature slightly. However, for fired operation the combustion-phasing retard that occurs with N_2 addition also lowers the wall temperature. Analysis of the data shows that this wall cooling almost perfectly counteracts the effect of slightly lower C_v for N_2. Consequently, N_2 addition does not change the compressed-gas temperature significantly and can be regarded as a way to isolate the $[O_2]$ effect on autoignition.

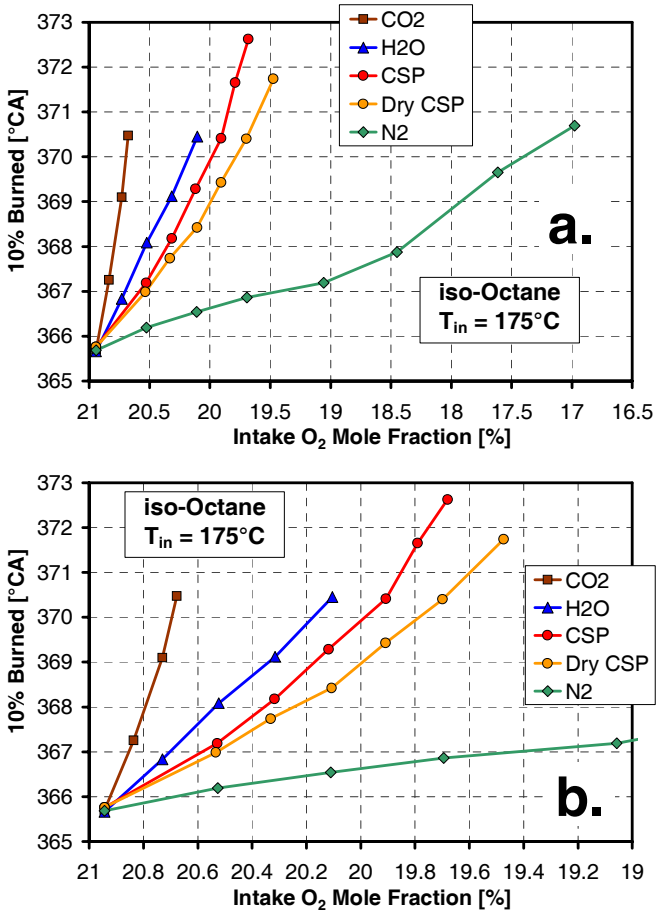

Figure 13. Effect of addition of CSP and constituents on CA10 for iso-octane. T_{in} = 175°C.

effect is relatively weak compared to the thermodynamic cooling. Furthermore, the order of the data sets follows well what could be expected from the thermal effect shown in Fig. 11. This indicates that for iso-octane, no other factors than [O_2] and thermodynamic cooling need to be considered to explain the position and relative order of the plotted data sets.

For better understanding, Fig. 14 demonstrates how the [O_2] effect and the thermodynamic-cooling effect lead to different charge-temperature histories for the same amount of autoignition timing retard. The temperature trace with the most advanced hot ignition is the baseline point with air dilution only. The other two temperature traces represent two different ways the autoignition can be retarded. When 1.3% of the air is replaced with CO_2, [O_2] drops only slightly to 20.7% while CA10 retards significantly from 365.7°CA to 370.4°CA. This retard is caused primarily by the lower compressed-gas temperature, as Fig. 14 shows. This thermal retard is analogous to lowering T_{in}. On the other extreme, replacing 19% of the air with N_2 leads to the same retard of CA10 without a significant change of the compressed-gas temperature in the 350 - 355°CA range. The heat-release commences at 355°CA for the baseline case, but the onset is retarded to beyond 360°CA for the N_2 case due to the lower [O_2]. This exemplifies autoignition retard due to chemical effects.

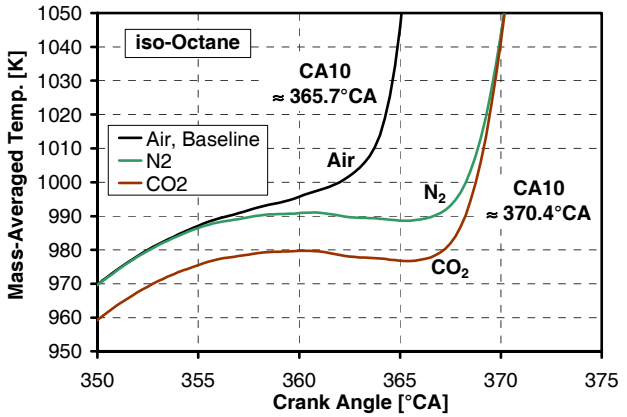

Figure 14. Illustrating the influence of the [O_2] effect and the thermodynamic cooling effect on the temperature for hot ignition. [O_2] = 17.0% for the N_2 case, and [O_2] = 20.7% for the CO_2 case.

COMBUSTION RETARD FOR PRF80

Figure 15 shows the effects of addition of CSP, dry CSP and the individual CSP constituents for PRF80. First, it can be observed that N_2 has a substantially stronger effect for PRF80 than it had for iso-octane. The sensitivity of CA10 to N_2 addition is almost as strong as it is to CSP. This shows that the [O_2] effect is much more pronounced for PRF80. Analysis of the data indicates that the higher [O_2] sensitivity is associated with the presence of LTHR for PRF80. The explanation has two parts:

First, as Fig. 16 exemplifies, PRF80 has LTHR in the 337 – 350°CA range. This LTHR accelerates the temperature rise and makes PRF80 undergo hot ignition at about the same crank angle as iso-octane and gasoline, despite a much lower T_{in}, as discussed in conjunction with Fig. 6. If the HRR during the LTHR phase decreases with lower [O_2], this would lead to lower compressed-gas temperatures and delayed hot ignition. In fact, the data show that this is the case. Figure 15a plots the temperature rise during the period of LTHR for various amounts of N_2 addition. It is clear that the total amount of LTHR is significantly reduced by the lower [O_2]. In fact, the percentage reduction of the LTHR is actually greater than Fig. 15a suggests since the piston compression accounts for a temperature rise of roughly 105 K in the 335 – 352°CA period.

The second part of the explanation relates to the indirect influence of LTHR on the hot ignition. The data also show that the transition into hot ignition is suppressed by the lower [O_2]. Figure 17 illustrates this for PRF80. The two cases plotted are chosen to have the same post-LTHR temperature, which is 920K at 355°CA. Despite the higher C_v for CO_2, this case has a more rapid temperature rise, which leads to an earlier onset of the main combustion[7]. The N_2 case suffers from the fact that

[7] It can be noted that CO_2 is effectively an inert species at the temperature levels prevailing during the autoignition processes [25,26].

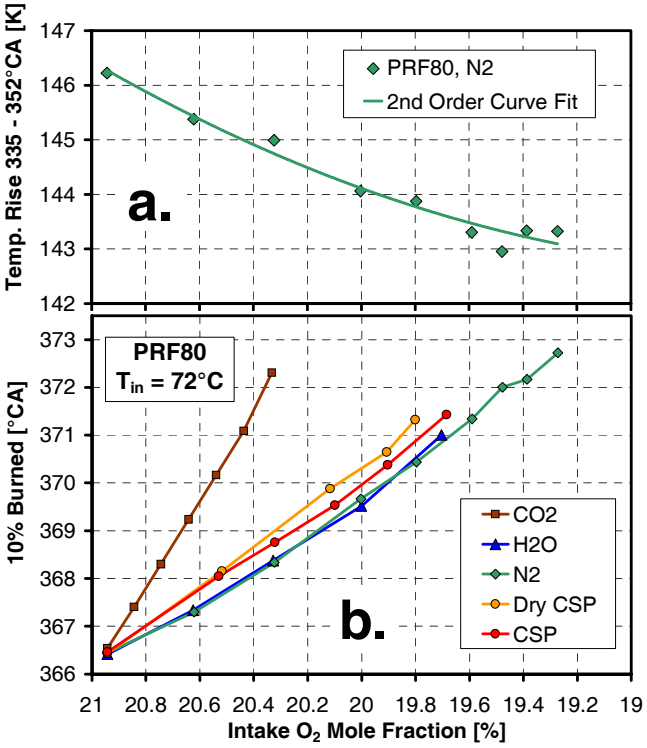

Figure 15. Effect of addition of CSP and constituents on CA10 for PRF80. Also, the temperature rise during the LTHR period is plotted for N_2. T_{in} = 72°C.

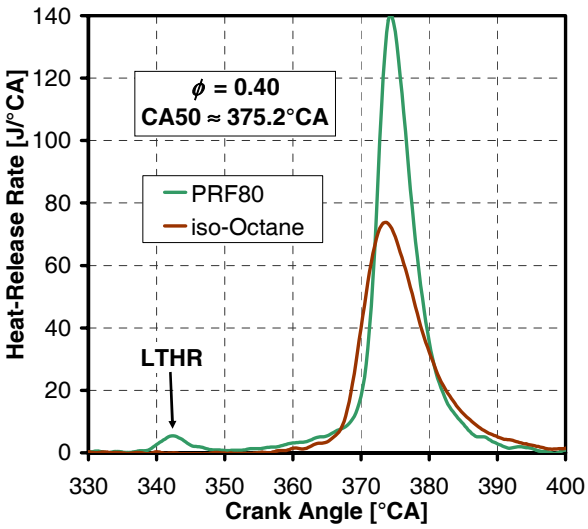

Figure 16. Comparison of HRR for PRF80 and iso-octane. The LTHR is clearly visible for PRF80 in the 336 - 351°CA range. 1.3% CO_2 addition for iso-octane, corresponding to the temperature trace in Fig. 14. 6.5% N_2 addition for PRF80, corresponding to the data point with $[O_2]$ = 19.6% in Fig. 15.

its $[O_2]$ is 1.4% lower than the CO_2 case (see legend of Fig. 17), so the hot ignition occurs late. This effect of $[O_2]$ on the hot ignition process is similar to that of iso-octane, as demonstrated in Fig. 14. However, the hot ignition has more than double the sensitivity to $[O_2]$ for PRF80 compared to iso-octane. The shift of hot ignition due to changes of $[O_2]$ is similar for Figs. 14 and 17 while the

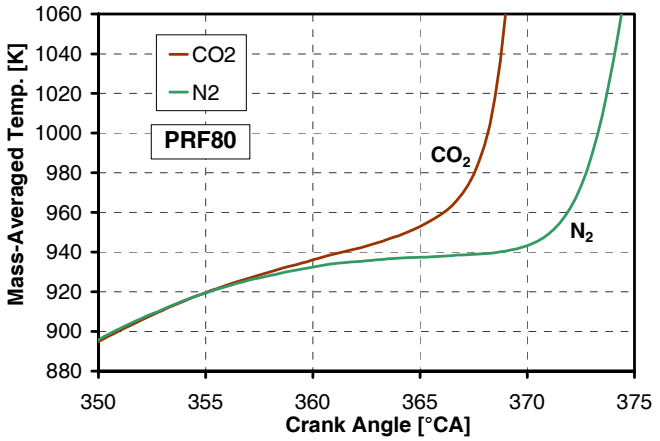

Figure 17. The effect of $[O_2]$ on timing of hot ignition for two cases with the same post-LTHR temperature. $[O_2]$ = 20.7% for the CO_2 case, and $[O_2]$ = 19.3% for the N_2 case. PRF80.

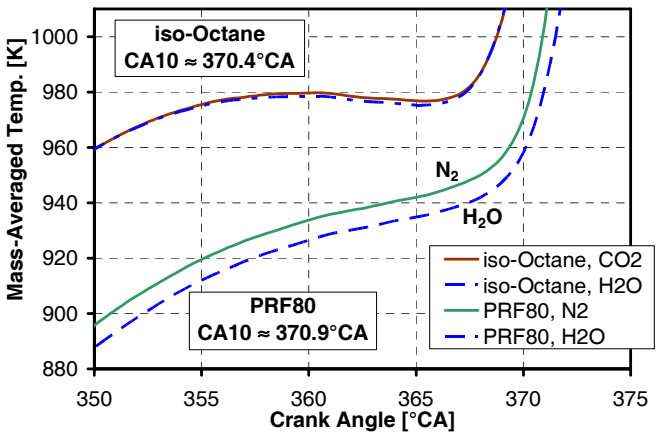

Figure 18. The effect of H_2O on the temperature for hot ignition. $[O_2]$ = 19.7% for both PRF80 temperature traces. $[O_2]$ = 20.7% for the CO_2 case with iso-octane, and $[O_2]$ = 20.1% for the H_2O case.

change of $[O_2]$ is 3.7% for the iso-octane case but only 1.4% for the PRF80 case. This higher $[O_2]$ sensitivity of the hot ignition is attributed to the presence of LTHR, which is known to significantly change the chemistry leading up to hot ignition [19,20].

The strong $[O_2]$ effect should be present for all gases. Therefore, the thermodynamic cooling caused by gas components with C_v higher than air would be expected to cause additional autoignition retard. Contrary to this expectation, Fig. 15b shows that H_2O addition causes exactly the same retard as N_2. Without further analysis of the data, this would be confusing. However, by studying the temperature traces, a second chemical effect was identified. This is illustrated in Fig. 18, which shows two PRF80 cases, one with 6% N_2 and the other with 6% H_2O. Since $[O_2]$ = 19.7% for both cases, the retarding effect of lower $[O_2]$ is expected to be the same. However, the higher C_v of H_2O leads to reduced compressed-gas temperatures near TDC, as expected. Despite this, the hot ignition occurs at the same crank angle, in agreement with Fig. 15b. This shows that H_2O

enhances the early reactions leading to the main hot ignition in such a way that the temperature required for thermal run-away is reduced by the same amount as the cooling effect of H_2O.

Now that the enhancing effect of H_2O has been identified, it is possible to explain the order of the PRF80 curves in Fig. 15b. For example, dry CSP has a slightly more retarding effect than CSP despite its lower C_v. This is the opposite behavior of iso-octane, and can be explained by the enhancing effect of H_2O present in CSP that occurs for PRF80 but not for iso-octane. CO_2 still has the strongest retarding effect due to its high C_v.

While Figs. 15b and 18 together show the enhancing effect of H_2O for PRF80, no such effect was needed to explain the behavior of iso-octane (Fig. 13). Indeed, analysis of temperature traces shows that the enhancing effect of H_2O is much smaller for iso-octane. This is illustrated in Fig. 18. The two iso-octane traces have similar $[O_2]$ and the resulting combustion-phasing retard is primarily caused by the thermodynamic cooling of CO_2 and H_2O, respectively. As can be seen, the temperature for which thermal run-away occurs is only a line width lower for the H_2O case. This indicates a very weak enhancing effect of H_2O for iso-octane.

COMBUSTION RETARD FOR GASOLINE

Figure 19 shows the effects of addition of CSP, dry CSP and individual constituents for gasoline. Compared to the other single-stage ignition fuel, iso-octane (Fig. 13), gasoline is only about half as sensitive to reductions in $[O_2]$ within the range plotted, as indicated by the nearly-horizontal N_2 curve. Another difference is the close spacing and order of the trends with CSP, dry CSP, and H_2O. As can be seen, dry CSP has a slightly stronger retarding effect than CSP. This is analogous to that of PRF80, as plotted in Fig. 15b. This indicates that H_2O has an enhancing effect on the hot ignition for gasoline as well. Indeed, examination of the temperature traces shows that this is the case. However, as illustrated in Fig. 20, the effect is much weaker than for PRF80. (Compare to Fig. 18.) Simply looking at the relative steepness of the curves in Fig. 19, it may seem strange that dry CSP has a slightly stronger retarding effect than CSP, given that the H_2O line is steeper than dry CSP (compare to Fig. 15). This could be explained by arguing that the enhancing effect of H_2O addition is non-linear. For example, going from dry CSP to CSP leads to a slight increase of both $[H_2O]$ and C_v. At this low concentration the chemical enhancement of the autoignition due to the H_2O is greater than the thermodynamic cooling effect, causing CA10 to be slightly less retarded. However, going from CSP to H_2O leads to a substantially larger increase of both $[H_2O]$ and C_v. Since CA10 now becomes significantly more retarded, this suggests that the enhancing effect of H_2O begins to saturate so that it no longer fully compensates for the lower compressed-gas temperature resulting from the increased C_v.

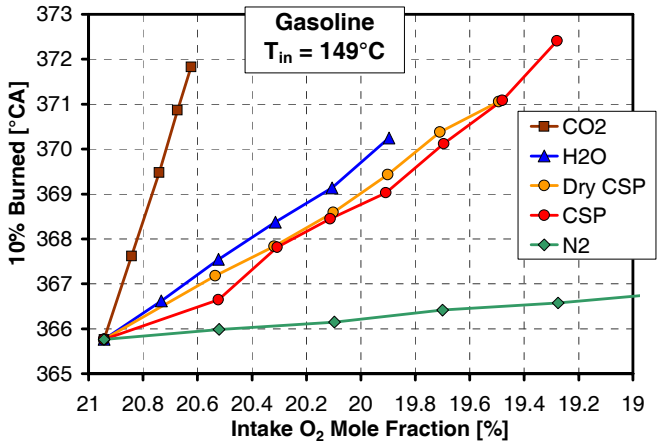

Figure 19. Effect of addition of CSP and constituents on CA10 for gasoline. T_{in} = 149°C.

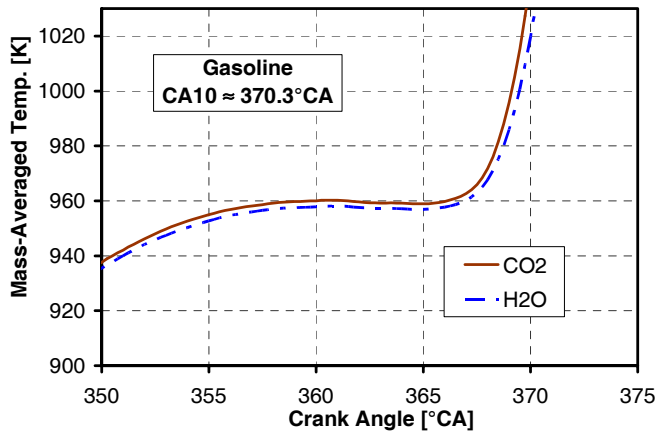

Figure 20. The effect of H_2O on the temperature for hot ignition of gasoline. $[O_2]$ = 20.7% for the CO_2 case and $[O_2]$ = 19.9% for the H_2O case.

COMPARING THERMAL AND $[O_2]$ SENSITIVITIES

Up until this point three mechanisms responsible for the changes in autoignition timing have been identified and discussed. These are:

1. C_v effect (thermodynamic – retarding).
2. O_2-concentration effect (chemical – retarding).
3. H_2O effect (chemical – enhancing).

The H_2O effect has already been compared directly for iso-octane, PRF80 and gasoline, so no more analysis of the H_2O effect will be presented.

Thermodynamic C_v effect - To fully understand why the fuels respond differently to CSP addition (Fig. 8) it is beneficial to compare the fuels in terms of their sensitivity to the thermodynamic cooling of EGR. To minimize the retarding effect of $[O_2]$, it is best to compare the response for CO_2, which is the gas that gives the least reduction of $[O_2]$ for a given amount of cooling. This comparison is shown in Fig. 21. As can be seen, gasoline and iso-octane show significantly higher sensitivity to the reduced compressed-gas temperature than PRF80 and PRF60 do. The reason for the

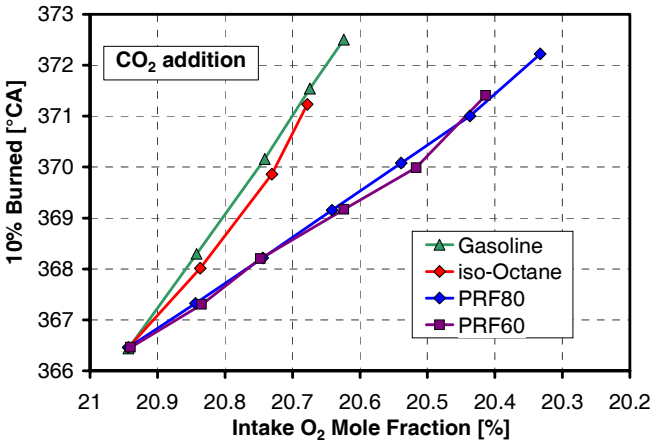

Figure 21. Comparing the retard of hot ignition due to the predominantly charge-cooling effect of CO_2. The PRF60 data set shifted 6.1% to facilitate direct comparison of the fuels.

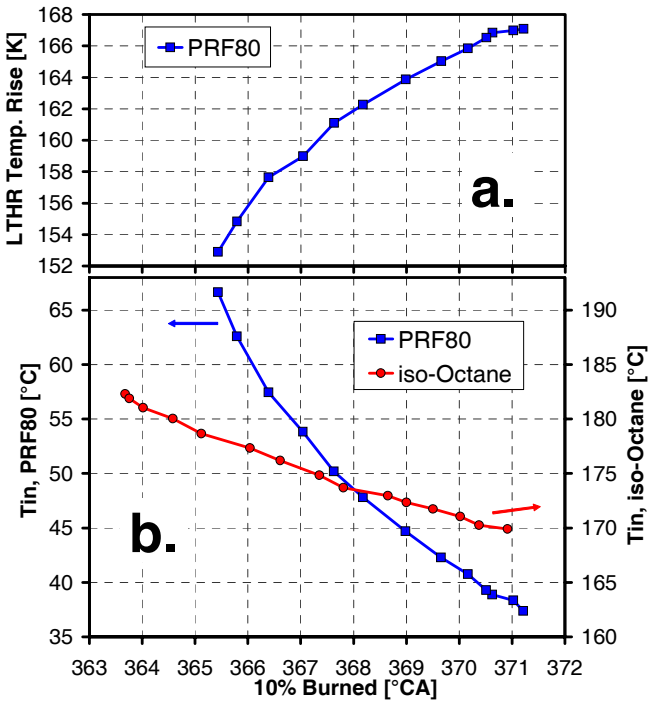

Figure 22. T_{in} required to achieve a certain CA10 for iso-octane and PRF80. No EGR. The temperature rise during the 335 – 352°CA range is also plotted for PRF80.

difference can be attributed to the presence of LTHR for PRF80 and PRF60, and the explanation has two components: 1) Lower compressed-gas temperature leads to more LTHR. As explained in Ref. [12], this happens because a reduction of the gas temperature leads to a delayed onset of LTHR, at which point the in-cylinder pressure is higher. 2) The presence of LTHR leads to a higher temperature-rise rate prior to hot ignition. This can be seen by comparing the curves for PRF80 against those of iso-octane in the 350 – 365°CA range in Fig. 18. Because of the higher temperature-rise rate for PRF80, a larger change of the gas temperature is required to shift the crank angle where the temperature exceeds the temperature for hot ignition. This is discussed in more depth in Ref. [12]. Thus, for a given change in compressed-gas temperature, the two-stage ignition fuels will experience less shift in CA10. This explains why the two-stage ignition fuels are less sensitive to the thermodynamic cooling effect. Finally, it is noteworthy that a similarly low sensitivity of autoignition timing to CO_2 addition for a two-stage ignition fuel was observed by Shudo *et al.* [26], who operated their HCCI engine on a blend of dimethylether (DME) and hydrogen.

The lower thermal sensitivity of the two-stage ignition fuels also has implications for the combustion-phasing control of the engine. Figure 22b shows how T_{in} has to be adjusted to achieve a certain CA10 for both iso-octane and PRF80. In agreement with the arguments above, it can be observed that significantly larger changes of T_{in} are required to achieve a certain shift of CA10 for PRF80. Figure 22a shows how the amount of LTHR increases with a reduction of T_{in}, thus counteracting the effect of lower T_{in} on CA10.

[O_2] reduction effect - Figure 23 compares the sensitivities of the four fuels to the predominantly oxygen-reducing effect of N_2 addition. The two-stage ignition fuels, PRF60 and PRF80, stand out with significantly higher sensitivity to the reduction of [O_2]. As discussed in conjunction with Figs. 15a and 17, this happens due to a combination of a reduction of LTHR and a suppression of the reactions leading to hot ignition. Gasoline represents the other end of the spectrum and shows very low sensitivity to moderate reductions of [O_2]. From the result presented in Fig. 23 it may tempting to suggest that all two-stage ignition fuels are sensitive to [O_2]. This could be true for traditional fuels, however, a recent study by Shudo *et al.* [26] shows that the LTHR of DME is insensitive to changes of the O_2 concentration in the 20.95 – 18.6% range. On the other hand, this insensitivity could possibly be explained by DME's very different molecular structure, which likely makes its low-temperature chemistry different from that of the longer-chain *n*-heptane.

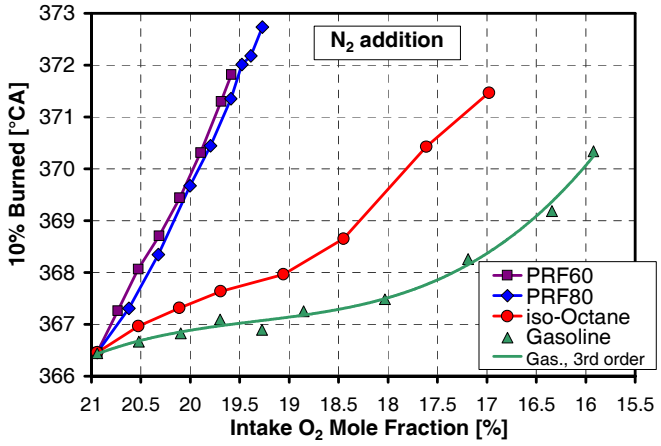

Figure 23. Comparing the retard of hot ignition due to the predominantly oxygen-reducing effect of N_2. The PRF60 data set shifted 6.1% to facilitate direct comparison of the fuels.

EXPLAINING CSP TRENDS

After the various mechanisms associated with the components of CSP have been identified, it is possible to explain the trends with CSP addition. Overall, the differences between the fuels, as plotted in Fig. 8, is smaller than the responses to the individual components. Both the single-stage and two-stage ignition fuels are affected by the three underlying mechanisms. While the single-stage fuels are more sensitive to the thermodynamic cooling effect of CSP, the two-stage ignition fuels are more sensitive to the [O_2] reduction effect. H_2O enhances the hot ignition substantially for the two-stage fuels, while this effect is less pronounced for both gasoline and iso-octane. The combined effect of these underlying mechanisms produces a similar response to CSP addition for the different fuels. Gasoline stands out somewhat with a lower sensitivity, which can be explained by its exceptionally low [O_2] sensitivity combined with a modest H_2O enhancing effect.

COMBUSTION RETARD WITH REAL EGR

Figure 24 compares the retarding effect of CSP with that of real EGR for iso-octane, gasoline, and PRF80. For the single-stage ignition fuels, real EGR clearly has a weaker retarding effect compared to CSP. However, for the two-stage ignition fuel PRF80, real EGR has a stronger retarding effect, at least beyond a certain degree of [O_2] reduction by EGR addition. The difference between CSP and real EGR is the presence of trace species that stem from incomplete combustion. At these high loads, the trace species originate primarily from the piston-ring crevice, which is a source of unburned fuel, and the thermal boundary layer which produces partially oxidized fuel and CO [27]. With increasing EGR rate, the concentrations of these species in the intake system go up rapidly, as shown in Fig. 25. This happens partly because a larger fraction of the incoming gases are EGR, but also because the retarded combustion phasing leads to less complete combustion.

Full analysis of the chemical effects of all the different species present in the exhaust gas is beyond the scope of this study. However, the net result on the ignition is clear from Fig. 24. The single-stage fuels iso-octane and gasoline see an enhancement of the autoignition from these species. This may not be too surprising since both iso-octane and gasoline have high resistance to autoignition, and it appears plausible that addition of a whole range of different hydrocarbons opens up new pathways for autoignition to occur. On the other hand, PRF80 is already fairly reactive due to the straight-chain molecule *n*-heptane, and it could be that most molecules generated by incomplete combustion are somewhat less reactive than *n*-heptane. It should be noted that the combined residence time in the exhaust and intake systems is on the order of 20 seconds, so any "active radicals" are not expected to be present in the inducted gases. The results presented in Fig. 24 are consistent with findings regarding the influence of trapped residual

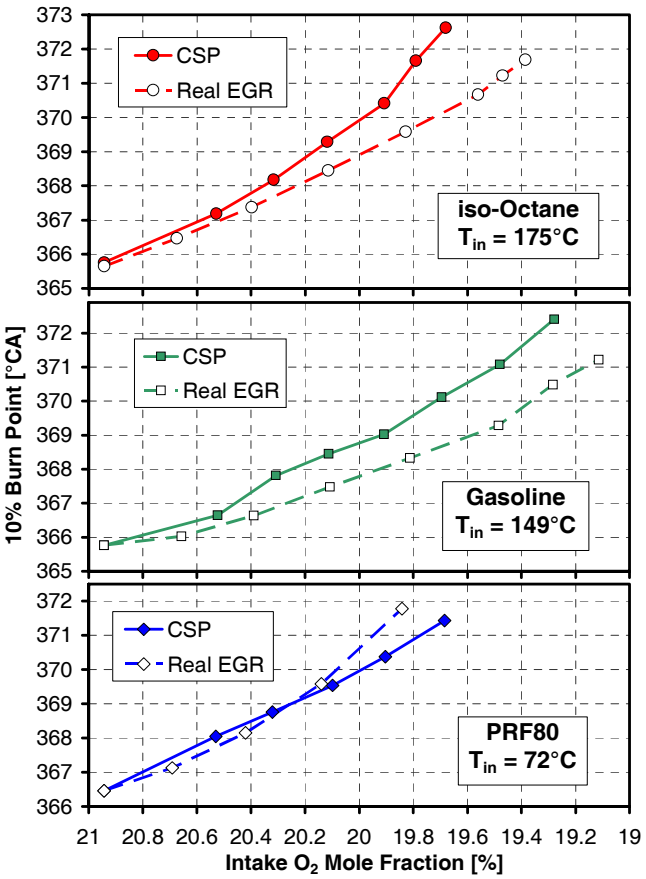

Figure 24. Comparison of simulated EGR (CSP) against real EGR.

gases on the autoignition of the following cycle, as reported in a recent study by the authors [12]. In that study, it was found that partial-burn products recycled from one cycle to the next enhance the autoignition for iso-octane, but suppress autoignition for PRF80. Formaldehyde was the only species identified to enhance autoignition for iso-octane but to suppress autoignition for PRF80. Formaldehyde has been found in significant quantities in HCCI exhaust [28]. It is also worth noting that LTHR has been found to produce substantial amounts of formaldehyde for PRF-fuels [29].

As Fig. 25 shows, CO is a fairly prevalent species. Dubreuil *et al.* [30] operated an HCCI engine with a 80/20 *n*-heptane/toluene blend that produced LTHR. They added up to 2000 ppm CO in the intake, but no significant effect on the autoignition could be observed. Based on this, CO would be expected to have insignificant effect on the autoignition timing. On the other hand, our chemical-kinetics modeling suggests that CO can have a substantial enhancing effect for PRF80. In contrast, the model showed no enhancing effect of CO for iso-octane. To clarify the role of CO, further studied are required.

Another trace species that is important to consider is NO, which has been shown to enhance the autoignition timing when added to the intake in low concentrations [30,31]. For the data in the current study, the gasoline case had up to 0.4 ppm NO in the intake, so this could

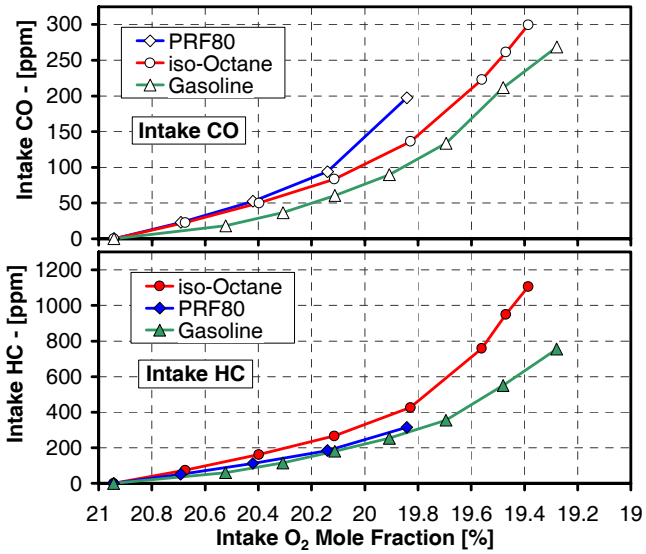

Figure 25. Intake HC and CO as a function of intake $[O_2]$ for operation with real EGR.

contribute to the enhancing effect of the trace species, as shown in Fig. 24. However, the NO concentration in the intake was less than 0.1 ppm for the iso-octane and PRF80 cases, so the enhancing effect of NO was probably very small for these fuels.

MODELING RESULTS

DATA INTERPRETATION

As explained in the section describing the modeling setup, a single-zone Senkin model was used to conveniently evaluate the performance of the detailed iso-octane and PRF mechanisms from LLNL. The goal is to compare the predicted changes in ignition timing as a result of EGR addition with those observed experimentally. Since the model is adiabatic, it can be thought of as representing the close-to-adiabatic core in the experiment. This hottest in-cylinder zone is where the combustion commences before it spreads to progressively colder zones. Multi-zone modeling shows

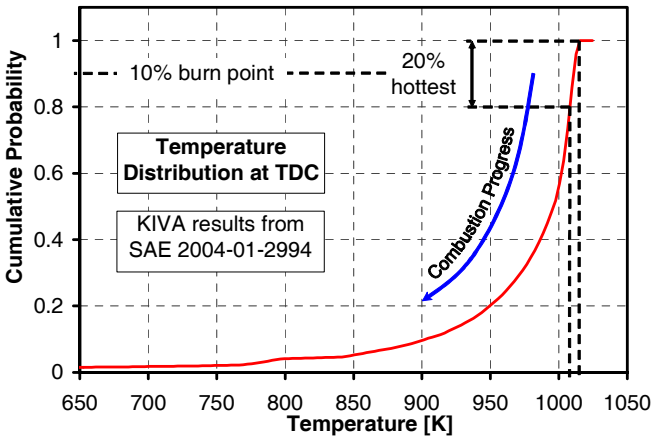

Figure 26. Rationale for comparing experimental 10% burn point against single-zone 50% burn point. The temperature distribution was computed with reactions disabled.

that for this C/F-mass ratio, the spread of the combustion occurs mainly by means of the combustion-induced pressure rise that compresses and heats not-yet-ignited zones. Furthermore, for this C/F-mass ratio, the local kinetics-controlled combustion rate is not the rate-limiting step for the overall combustion rate. As explained in Ref. [14], the thermal width of the charge in combination with the piston-expansion rate determines the combustion rate. Figure 26 shows an example of the cumulative mass probability of the in-cylinder temperature distribution, as reproduced from KIVA results of motored operation [15]. The combustion progresses from hotter to colder zones as noted in the graph. As also indicated in the graph, the hottest 20% of the compressed gas has a fairly uniform temperature (narrow horizontal width). The 50% burn point of this hottest zone corresponds roughly to CA10 of the overall combustion event. CA10 is also the burn point plotted in all experimental graphs in the previous sections. If the single-zone model is meant to reproduce this close-to-adiabatic core, it is sensible to compare the experimental CA10 against the 50% burn point for the model. This is the approach used below.

VALIDATION OF THERMODYNAMIC LIBRARY

Since EGR has significantly different thermodynamic properties from air, the ability of the model to correctly predict autoignition requires that the thermodynamic properties of all the gases be implemented correctly. To verify this, the model was configured to reproduce the experimental motored data shown in Fig. 11. To achieve the same compressed-gas pressure for the adiabatic model it was given a reduced CR of 12.7. To make the baseline $[O_2]$ = 20.95% point of the model match that of the experiment, the model values are extracted 6°CA earlier than the experiment (344°CA vs. 350°CA). The results of this exercise are shown in Fig. 27. As can be seen, the model does a good job of predicting the

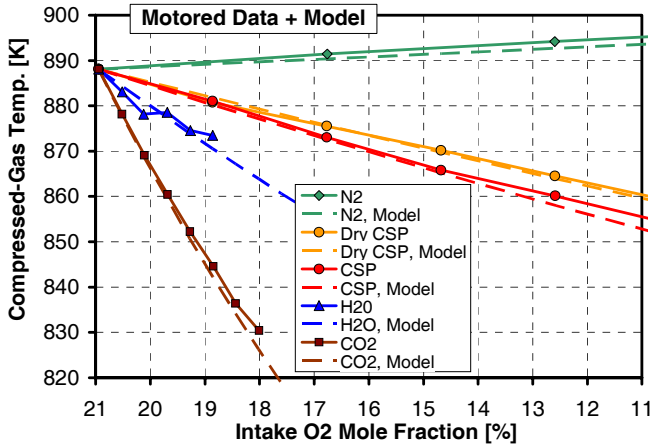

Figure 27. Evaluation of the thermodynamic treatment of the model. The experimental mass-averaged temperatures are computed from the pressure traces at 350°CA. The temperatures for the adiabatic model are extracted at 344°CA to match the experimental $[O_2]$ = 20.95% point.

changes in the compressed-gas temperature that occur when air is replaced with CSP, dry CSP, and the individual constituents. The thermodynamic library used was developed at LLNL [32]. Consequently, if model discrepancies are found when reproducing fired operation, those should be attributed to the chemical-kinetics treatment, not the thermodynamics.

EVALUATION OF CHEMICAL-KINETICS MECHANISMS

First, it should be noted that the PRF mechanism from LLNL exhibits less LTHR than that observed experimentally. Because of this, PRF40 was used for the simulations that correspond to experimental operation with PRF80 fuel. This problem with the LTHR is illustrated in Fig. 28. As can been seen, the experiment has a substantial amount of LTHR for PRF80. However, the model does not predict any LTHR when PRF80 fuel is used. (This discrepancy was also discussed in Ref. [5].) In fact, the *n*-heptane content needs to be increased significantly to create a rational amount of LTHR. Using PRF40, the model produces a substantial amount of LTHR. Although the peak HRR during the LTHR is higher, it also has a shorter duration. Integration of the HRR curves shows that the PRF40 fuel produces an amount of LTHR that is comparable to that of the experiment. Consequently, the BDC temperature required to establish the baseline operating point with only air dilution was similar to that of the experiment. Furthermore, it can be noted that the phasing of the LTHR peak lags that of the experiment.

Figure 29 compares the autoignition retard with CSP addition for iso-octane and PRF80. As can be seen, the model predicts too-low sensitivity for both iso-octane and PRF80. In addition, it indicates that PRF80 should have more retard than iso-octane for a given [O_2], which is opposite from the experimental results. To identify the causes for these discrepancies, Figs. 30 – 32 examine the performance for CO_2, N_2 and H_2O. (Note that the x-axis scales vary significantly between these figures.)

Figure 30 shows the effect of N_2 addition for iso-octane and PRF80. As can be seen, the model severely under

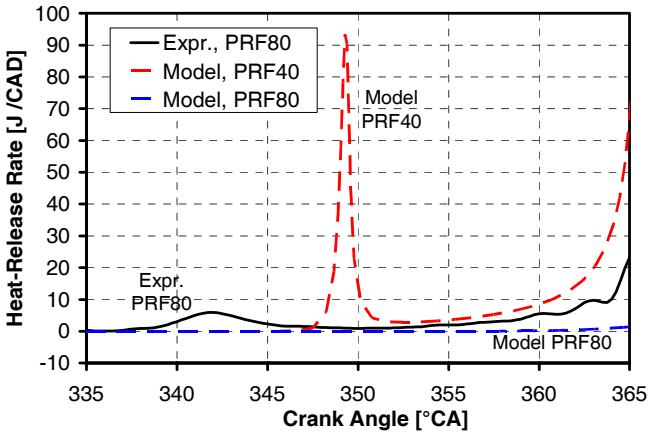

Figure 28. Rationale for using PRF40 to simulate the experimental PRF80 data sets.

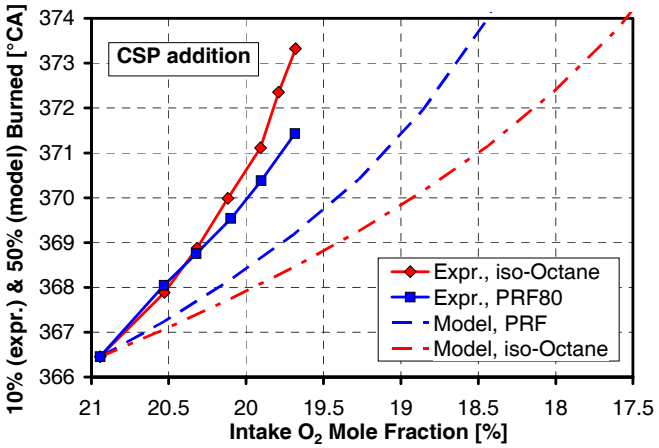

Figure 29. Evaluation of model performance for CSP addition.

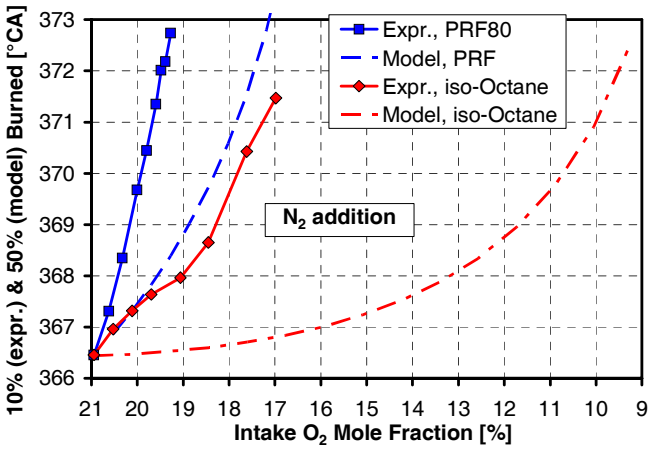

Figure 30. Evaluation of model performance regarding retard of hot ignition due to the predominantly oxygen-reducing effect of N_2.

predicts the [O_2] sensitivity for both fuels. This discrepancy can largely explain the problems with CSP addition, as plotted in Fig. 29. To its credit, the model shows that the two-stage ignition fuel (PRF80) has significantly higher [O_2] sensitivity than the single-stage ignition fuel (iso-octane). The too-low [O_2] sensitivity of the iso-octane mechanism has also been identified by He *et al.* [25].

As discussed above, addition of CO_2 gives the least reduction of [O_2] for a given amount of thermodynamic cooling. Therefore, CO_2 is a good species to evaluate the thermal sensitivities of both mechanisms. It can be noted that CO_2 is effectively an inert species at the temperature levels prevailing during the autoignition processes [25,26]. Figure 31 shows the result for iso-octane and PRF80. As can be seen, the model reproduces quite well the trend with PRF80. However, since we know from Fig. 30 that the [O_2] sensitivity is too low, the parallel curves in Fig. 31 mean that the thermal sensitivity of the model is somewhat too high for PRF80. Furthermore, Fig. 31 suggests that the thermal sensitivity is too low for the iso-octane model, but part of this discrepancy can be explained by the too-low [O_2] sensitivity. Rapid-compression studies by He *et al.* [25]

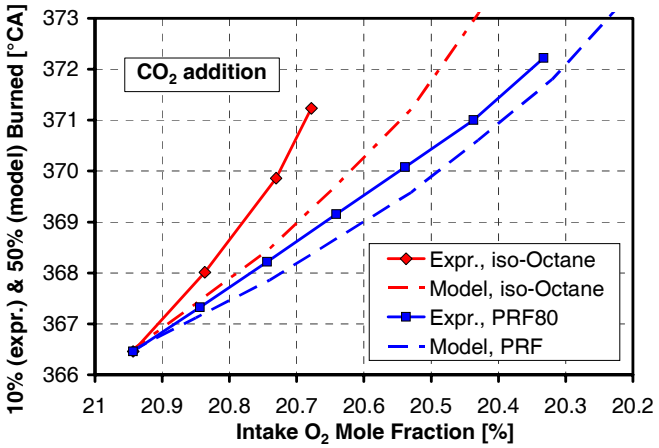

Figure 31. Evaluation of model performance regarding retard of hot ignition due to the predominantly charge-cooling effect of CO_2.

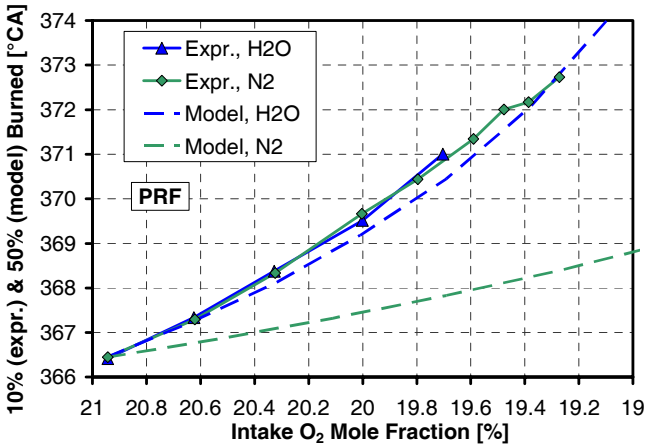

Figure 32. Evaluation of model performance. The non-overlapping dashed curves shows the too-weak ignition-enhancing effect of H_2O for the PRF mechanism used to simulate PRF80.

showed that the thermal sensitivity of the LLNL iso-octane mechanism was slightly lower than that found experimentally.

Enhancement of the autoignition reactions by H_2O was identified as an important mechanism for PRF80, as discussed in conjunction with Figs. 15b and 18. This effect is so strong that it compensates for the high C_v of H_2O and makes the H_2O and N_2 lines overlap in Fig. 15b. These two curves are reproduced in Fig. 32, along with the modeling results. The retarding effect of N_2 is less than observed experimentally, due to the too-weak $[O_2]$ effect as discussed above. However, the too-weak $[O_2]$ effect should also affect the H_2O result. Since the model curve for H_2O shows substantially more retard than the model curve for N_2, this means that the enhancing effect of H_2O in the model is less than observed experimentally.

Having gained these insights, the results in Fig. 29 can be re-evaluated. The model shows too-little sensitivity to CSP addition. The main reason for this is the too-low $[O_2]$ sensitivity for both fuels. In the case of PRF80, the too-high thermal sensitivity and the too-low enhancing effect of H_2O partly compensate for this and make the CSP prediction closer to the experiment than it would have been otherwise.

SUMMARY AND CONCLUSIONS

Exhaust gas recirculation (EGR) can be used beneficially to control combustion phasing in HCCI engines. For the gasoline and PRF fuels investigated here, EGR addition retards the start of combustion for a fixed T_{in} and C/F-mass ratio. However, the amount of retard is dependent on the specific fuel type and the kind of EGR - real EGR, simulated EGR (CSP), or dry CSP.

To clarify the reasons for these different trends, the underlying mechanisms were identified by conducting experiments with individual EGR constituents (N_2, CO_2, and H_2O). In addition, experiments were conducted with both real and simulated EGR. The mechanisms identified are:

1. Thermodynamic cooling effect due to high specific-heat capacity of CO_2 and H_2O. The single-stage ignition fuels, iso-octane and gasoline, are more sensitive to this retarding thermal effect than the two-stage ignition fuels, PRF80 and PRF60.

2. $[O_2]$ reduction effect, which is caused by the displacement of air by the EGR gases. This retarding effect is strong for the two-stage ignition fuels (PRF80 and PRF60) but quite weak for the single-stage fuels (iso-octane and gasoline). Gasoline showed the lowest sensitivity to $[O_2]$.

3. Enhancement of autoignition due to the presence of H_2O. This effect is strong for the two-stage PRF fuels, but much weaker for gasoline and iso-octane.

4. Enhancement or suppression of autoignition due to the presence of trace species such as unburned or partially-oxidized hydrocarbons, CO, and NO. The single-stage ignition fuels (iso-octane and gasoline) saw enhancement of autoignition due to these species, while PRF80, which has two-stage ignition, became more retarded.

In addition, the predictive capabilities of the detailed chemical-kinetics mechanisms for iso-octane and PRF from LLNL were evaluated. Comparison with motored data showed that the thermodynamic treatment of EGR is well implemented. Despite this, the model showed some significant discrepancies when configured to reproduce the retard of autoignition observed experimentally. The main problem for both mechanisms is too-low sensitivity to the reduction of $[O_2]$ associated with EGR, thus indicating an area where the mechanisms could be improved.

ACKNOWLEDGEMENTS

The authors would like to thank Lloyd Claytor, Kenneth St. Hilaire, Eldon Porter and Gary Hubbard for their dedicated support of the HCCI laboratory.

A part of the financial support for this investigation was provided by Aramco Services Company under WFO contract 083041026.

The work was performed at the Combustion Research Facility, Sandia National Laboratories, Livermore, CA. Financial support for establishing and operating the HCCI lab facility and for part of this investigation was provided by the U.S. Department of Energy, Office of FreedomCAR and Vehicle Technologies. Sandia is a multiprogram laboratory operated by the Sandia Corporation, a Lockheed Martin Company, for the United States Department of Energy's National Nuclear Security Administration under contract DE-AC04-94AL85000.

REFERENCES

1. Risberg, P., Kalghatgi, G., and Ångström, H.-E., "Auto-Ignition Quality of Gasoline-Like Fuels in HCCI Engines", SAE Paper 2003-01-3215, 2003.
2. Christensen, M., Johansson, B., Amnéus, P., and Mauss, F., "Supercharged Homogeneous Charge Compression Ignition", SAE Paper 980787, 1998.
3. Yao, M., Chen, Z., Zheng, Z., Zhang, B., and Xing, Y., "Effects of EGR on HCCI Combustion Fuelled with Dimethyl Ether (DME) and Methanol Dual-Fuels", SAE Paper 2005-01-3730, 2005.
4. Risberg, P., Kalghatgi, G., Ångström, H.-E., and Wåhlin, F., "Auto-Ignition Quality of Diesel-Like Fuels in HCCI Engines", SAE Paper 2005-01-2127, 2005.
5. Dec, J.E. and Sjöberg, M., "Isolating the Effects of Fuel Chemistry on Combustion Phasing in an HCCI Engine and the Potential of Fuel Stratification for Ignition Control", SAE Paper 2004-01-0557, 2004.
6. Kuo, T.-W., "Valve and Fueling Strategy for Operating A Controlled Auto-Ignition Combustion Engine," presented at the SAE Homogeneous Charge Compression Ignition (HCCI) Symposium, San Ramon, CA, Sept. 24-26, 2006.
7. Zhao, F., Asmus, T. W., Assanis, D. N., Dec, J. E., Eng, J. A., and Najt, P. M., Homogeneous Charge Compression Ignition (HCCI) Engines: Key Research and Development Issues, Society of Automotive Engineers, Warrendale, PA, 2003.
8. Cooper, B., Jackson, N., Penny, I., Truscott, T., Rawlins, D., and Seabrook, J., "Advanced Development Techniques for Delivering Low Emissions Diesel Engines", Proceeding of THIESEL 2006, pp. 267 – 280, 2006.
9. Sjöberg, M. and Dec, J.E., "Smoothing HCCI Heat-Release Rates using Partial Fuel Stratification with Two-Stage Ignition Fuels", SAE Paper 2006-01-0629, 2006.
10. Sjöberg, M. and Dec, J.E., "EGR and Intake Boost for Managing HCCI Low-Temperature Heat Release over Wide Ranges of Engine Speed", SAE Paper 2007-01-0051, 2007.
11. Sjöberg, M. and Dec, J.E., "Combined Effects of Fuel-type and Engine Speed on Intake Temperature Requirements and Completeness of Bulk Gas Reactions in an HCCI Engine", SAE Paper 2003-01-3173, 2003.
12. Sjöberg, M. and Dec, J.E., "Comparing Late-cycle Autoignition Stability for Single- and Two-Stage Ignition Fuels in HCCI Engines", Proceedings of the Combustion Institute, Vol. 31, pp. 2895–2902, 2007.
13. Sjöberg, M., Dec, J.E., and Cernansky, N.P., "Potential of Thermal Stratification and Combustion Retard for Reducing Pressure-Rise Rates in HCCI Engines, based on Multi-Zone Modeling and Experiments", SAE Paper 2005-01-0113, 2005.
14. Sjöberg, M. and Dec, J.E., "Effects of Engine Speed, Fueling Rate, and Combustion Phasing on the Thermal Stratification Required to Limit HCCI Knocking Intensity", SAE Paper 2005-01-2125, 2005.
15. Sjöberg, M., Dec, J.E., Babajimopoulos, A., and Assanis, D., "Comparing Enhanced Natural Thermal Stratification against Retarded Combustion Phasing for Smoothing of HCCI Heat-Release Rates", SAE Paper 2004-01-2994, 2004.
16. Aroonsrisopon, T., Foster D.E., Morikawa, T., and Iida, M., "Comparison of HCCI Operating Ranges for Combinations of Intake Temperature, Engine Speed and Fuel Composition", SAE Paper 2002-01-1924, 2002.
17. Dec, J.E. and Sjöberg, M., "A Parametric Study of HCCI Combustion – the Sources of Emissions at Low Loads and the Effects of GDI Fuel Injection", SAE Paper 2003-01-0752, 2003.
18. Lutz, A. E., Kee, R. J., and Miller, J. A., "Senkin: A FORTRAN Program for Predicting Homogeneous Gas Phase Chemical Kinetics with Sensitivity Analysis," Sandia National Laboratories Report No. SAND87-8248.
19. Curran, H. J., Gaffuri, P., Pitz, W. J., and Westbrook, C. K., "A Comprehensive Modeling Study of Iso-Octane Oxidation," *Combustion and Flame*, Vol. 129, pp. 253-280, 2002. www-cms.llnl.gov/combustion/combustion2.html
20. Curran, H. J., Gaffuri, P., Pitz, W. J., and Westbrook, C. K., "A Comprehensive Modeling Study of n-Heptane Oxidation," *Combustion and Flame,* Vol. 114, pp. 149-177, 1998.
21. Pitz, W. J., Lawrence Livermore National Laboratory, Personal Communication, 2003.
22. Heywood, J. B., Internal Combustion Engine Fundamentals, McGraw-Hill, New York, 1988.
23. Naik, C.V., Pitz, W.J., Sjöberg, M., Dec, J.E., Orme, J., Curran, H.J., Simmie, J.M., and Westbrook, C.K., "Detailed Chemical Kinetic Modeling of Surrogate

Fuels for Gasoline and Application to an HCCI Engine", SAE Paper 2005-01-3741, 2005.

24. NIST Chemistry WebBook, Standard Reference Database Number 69, June 2005 Release. http://webbook.nist.gov/chemistry/
25. He, X., Donovan, M.T., Zigler, B.T, Palmer, T.R., Walton, S.M., Wooldridge M.S., and Atreya A., "An Experimental and Modeling Study of iso-Octane Ignition Delay Times under Homogeneous Charge Compression Ignition Conditions", *Combustion and Flame,* Vol. 142, pp. 266-275, 2005.
26. Shudo T., Kitahara, S., and Ogawa, H., "Influence of Carbon Dioxide on Combustion in an HCCI Engine with the Ignition-Control by Hydrogen", SAE Paper 2006-01-3248, 2006.
27. Aceves S.M., Flowers, D.L., Espinosa-Loza, F., Martinez-Frias, J., Dec, J.E., Sjöberg, M., Dibble R.W., and Hessel, R.P., "Spatial Analysis of Emissions Sources for HCCI Combustion at Low Loads Using a Multi-Zone Model", SAE Paper 2004-01-1910, 2004.
28. Kaiser, E.W., Maricq, M.M., Xu, N., and Yang, J., "Detailed Hydrocarbon Species and Particulate Emissions From An HCCI Engine as a Function of Air-Fuel Ratio", SAE Paper 2005-01-3749, 2005.
29. Särner, G., Richter, M., Aldén, M., Hildingsson, L., Hultqvist, A., and Johansson, B., "Simultaneous PLIF Measurements for Visualization of Formaldehyde- and Fuel- Distributions in a DI HCCI Engine", SAE Paper 2005-01-3869, 2005.
30. Dubreuil, A., Foucher, F., Mounaim-Rousselle, C., "Effect of Chemical Components, Amount and Temperature of the Exhaust-Gas-Recirculation on the Combustion Development in HCCI Mode", Proceeding of THIESEL 2006, pp. 629 – 631, 2006.
31. Risberg, P., Johansson, D., Andrae, J., Kalghatgi, G., Björnbom, P., and Ångström, H.-E., "The Influence of NO on the Combustion Phasing in an HCCI Engine", SAE Paper 2006-01-0416, 2006.
32. www-cms.llnl.gov/combustion/combustion2.html